SSRG International Journal of Electrical and Electronics Engineering
ISSN: 2348-8379/ https://doi.org/10.14445/23488379/IJEEE-V11I3P126

Volume 11 Issue 3, 308-323, March 2024

Original Article

Efficiency and Performance Optimization of Non-Ideal Synchronous Buck Converter Using MOMI Tuned PID Controller for Voltage Mode Control

Prasanna Bagdalkar[1], Layak Ali[2]

[1,2]*Department of ECE, School of Engineering, Central University of Karnataka, Karnataka, India.*

[1]*Corresponding Author : prasannabagdalkar@gmail.com*

Received: 18 January 2024 Revised: 13 February 2024 Accepted: 15 March 2024 Published: 25 March 2024

Abstract - *This paper investigates the performance of three different methods of tuning a PID controller-MOMI, Harriot, and Good-Gain for a non-ideal synchronous buck converter. The mathematical model is derived through state space averaging and small signal modelling techniques for accurate and realistic assessment of the tuning methods. The Simscape tool of MATLAB/Simulink facilitates closed-loop simulation. The results indicate that the MOMI method outperforms in terms of transient response and steady-state error under significant input voltage variations (up to 50%), demonstrating minimal overshoot (16%), quick settling time (2.7ms), and zero steady-state error. Also, under dynamic load conditions, the MOMI approach consistently demonstrates decreased overshoot in the output voltage and faster convergence to the steady-state value, signifying improved transient performance. Furthermore, the MOMI method shows the lowest error signal in tracking output reference voltage changes, indicating its superior tracking capability and rapid adaptation. This research contributes to the field of control systems by advancing the understanding of PID controller performance under different variations. It highlights the effectiveness of the MOMI method in achieving optimal performance. The study validates the critical role of tuning methods in the design of optimized PID controllers that strike a delicate balance between efficiency and performance.*

Keywords - *DC-DC converter, Damped oscillation method, Magnitude Optimum Multiple Integration method, Proportional Integral Derivative (PID) controller, Non-ideal synchronous buck DC-DC converter.*

1. Introduction

The synchronous buck converter, a key component in power electronics, is a major element in managing and converting energy. Its adaptability and efficiency make it a common choice for various uses, from powering digital devices and electric vehicles to renewable energy systems. Its ability to deliver high currents while reducing power loss has made it an essential element in consumer electronics.

The growing need for energy efficiency in DC/DC converters, especially in mass-produced consumer electronics, has spurred the development of cost-effective synchronous rectification solutions. These converters are thought to offer substantial efficiency improvements compared to their non-synchronous counterparts [1].

The importance of efficiency is further highlighted by strict energy regulations and green initiatives. In the present era, designers aim to enhance converter efficiency without increasing costs, particularly in high-volume applications, where saving even a single watt can result in substantial energy savings.

However, despite the efficiency and versatility of synchronous buck converters, achieving optimal control for peak performance demands using a non-ideal model of the synchronous converter in the design and modelling of the controller due to the following reasons.

Firstly, ideal models neglect voltage drops caused by real-world components like switch and MOSFET resistances, inductor Equivalent Series Inductance (ESL), and capacitor Equivalent Series Resistance (ESR). This discrepancy between predicted and actual voltage becomes particularly evident under transient and load variations, leading to suboptimal performance [1, 2].

Secondly, ideal models overlook the additional poles and zeros introduced by non-ideal components, which influence transient response and stability. This can result in a sluggish response, overshooting, even instability under certain conditions, and issues ideal models would not predict.

Thirdly, assuming perfect efficiency, ideal models fail to account for power losses due to conduction and switching,

hindering accurate evaluation of energy consumption and thermal management [3]. Therefore, due to the critical impact of model accuracy on controller effectiveness, non-ideal models become indispensable tools for achieving optimal performance in synchronous buck converters.

In the research area of power electronics, the Proportional-Integral-Derivative (PID) controller plays a key role in maintaining system stability and performance. Its significance is particularly noticeable in the context of synchronous buck converters, where PID controllers are indispensable for achieving precise voltage mode control. However, the effectiveness of these controllers relies heavily on their tuning, i.e., a process that involves adjusting the integral gain, derivative gain and proportional gains to optimize system performance [4].

While designing a PID controller for a synchronous buck converter is crucial, relying solely on a non-ideal model can limit its effectiveness. Effective tuning methods are essential to optimize the converter's performance. The effectiveness of PID controllers extends beyond their design and is significantly influenced by their tuning. Much like a finely tuned instrument resonates with flawless harmony, a precisely tuned PID controller can enhance the performance of a non-ideal synchronous buck converter with remarkable accuracy [5]. Therefore, meticulously tuning PID controllers unlocks the hidden potential of synchronous buck converters.

This research paper addresses this gap by proposing a novel approach utilizing a Magnitude Optimum Multiple Integrations (MOMI) tuned PID controller for synchronous buck converter voltage mode control. MOMI tuning offers a systematic method for optimizing PID parameters, potentially leading to significant improvements compared to conventional tuning techniques.

Unlike traditional methods that may struggle with non-ideal models, MOMI tuning leverages a more accurate representation of the converter, enabling superior control performance. This can translate to benefits like faster transient response, enhanced disturbance rejection, and potentially even efficiency gains.

The literature review of PID controller tuning is vast and diverse, with a multitude of methods developed and refined over the years. In this paper, the literature review is broadly classified into two categories for a more structured and comprehensive understanding. Firstly, the classical methods represent the traditional techniques that have been used since the inception of PID controllers, which include the following. The Ziegler-Nichols method is a simple and widely used tuning method based on open-loop step response analysis [6].

While this method can be a helpful initial step in the tuning process, it may not be the most effective approach for systems exhibiting pronounced non-linear characteristics or behaviour that change over time. There are different variations of this method, such as closed-loop, Modified Ziegler-Nichols, and tuning from frequency response, which offer more flexibility and can potentially handle non-idealities better. However, these methods may have higher computational complexity, making them less suitable for real-time applications [7].

The Cohen-Coon method offers direct design formulas based on desired closed-loop characteristics like rise time and settling time [8]. This makes it a good choice for systems where specific performance objectives are important. However, like the ZN method, it may struggle with nonlinearities and time-varying behaviour. The computational complexity of the Cohen-Coon method is comparable to that of the ZN method [5].

The CHR method combines the ZN and Cohen-Coon methods for improved robustness and disturbance rejection [9]. This makes it a good choice for systems with significant non-idealities. However, the CHR method can be more computationally complex than the ZN or Cohen-Coon methods, which may make it less suitable for real-time applications [10].

Modern Methods: With the advent of new technologies and computational power, more sophisticated and efficient tuning methods have emerged. These modern methods often provide better performance and robustness compared to classical methods. Model Predictive Control (MPC) provides optimal control actions based on a system model and future predictions [11].

It can handle nonlinearities and uncertainties effectively, making it a good choice for non-ideal synchronous buck converters. MPC can meet specific performance objectives like settling time, overshoot, and disturbance rejection. However, the computational complexity of MPC is high, especially for real-time applications, due to the need to resolve an optimization issue during a single iteration. Fuzzy Logic Control (FLC) introduces human-like decision-making capabilities to handle nonlinearities and uncertainties, achieving robust performance in complex systems [12].

FLC can handle non-idealities in synchronous buck converters and can meet specific performance objectives. The computational complexity of FLC is relatively low compared to MPC, making it appropriate for practical applications. However, the design and tuning of FLC can be challenging due to the lack of systematic design methods [12].

Adaptive PID Control automatically adjusts PID gains online based on system dynamics and operating conditions, enhancing performance and robustness [13]. It can handle non-idealities in synchronous buck converters and can meet

specific performance objectives. The computational complexity of Adaptive PID Control is comparable to traditional PID control, making it appropriate for Practical applications. However, the performance of Adaptive PID Control rests on the accuracy of the derived system model and the adaptation algorithm [13].

The PID controller tuning method presented in this research paper is the Magnitude Optimum Multiple Integrations (MOMI) method, which has emerged as a recent advancement offering a compelling combination of performance, robustness, flexibility, and computational efficiency. It offers several key advantages over both classical and modern methods: Unlike some classical methods, MOMI ensures a non-oscillatory response for a wide range of systems, promoting stability in critical applications [14].

MOMI effectively addresses nonlinearities and time-varying behaviour, making it well-suited for non-ideal systems like synchronous buck converters, a common challenge in power electronics. The MOMI method optimizes the frequency response for superior disturbance rejection and set-point tracking, potentially surpassing the capabilities of classical methods.

The rest of the research paper is structured as follows: the mathematical modeling of plant, i.e., synchronous buck converter with non-idealities, is derived in section 2. The significance of the Proportional Integral Derivative (PID) controller is represented in both time and frequency domains in section 3. The Magnitude Optimum Multiple Integration (MOMI) tuning method is thoroughly described in section 4, which also includes a comparison with the Harriot and Good-Gain methods. The simulation results of the non-ideal synchronous buck converter subjected to dynamic changes in input, output, and reference are represented in section 5. Finally, a comprehensive interpretation of the complete paper is provided in section 6.

2. Mathematical Modelling of Non-Ideal Synchronous Buck DC-DC Converter

This section presents mathematical modelling of a typical synchronous buck converter, considering all parasitic losses due to the imperfect characteristics of physical components such as the inductor and capacitor [15]. The synchronous buck converter comprises a power stage and an output filter stage. In the power stage, two MOSFET switches, Q_H and Q_L, are connected in a half-bridge arrangement, as depicted in Figure 1.

Unlike traditional buck converters, this configuration utilizes a second MOSFET as the low-side switch instead of a power diode to enhance efficiency for low-power applications. In this configuration, MOSFETs Q_H and Q_L are switched alternately to each other, hence the name "synchronous buck converter". This synchronous switching action connects the output filter stage to a square-wave-like input voltage signal having a frequency equal to the converter switching frequency f_{sw}, with duty cycle D equal to the conduction time t_{on} of MOSFET Q_H divided by the total switching period T_{sw}, i.e., $D = t_{on}/T_{sw}$.

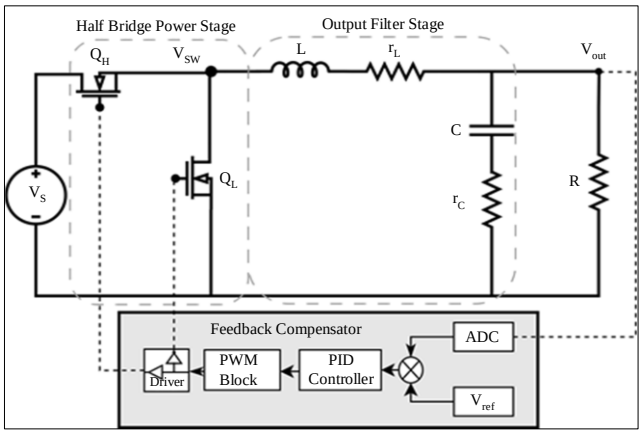

Fig. 1 Simplified circuit diagram of a synchronous non-ideal buck converter with PID controller for voltage mode control

The output stage of a synchronous buck converter includes energy storage elements like an inductor and capacitor. It acts as a low-pass filter of the second order, constructing a steady DC output voltage. The non-ideal synchronous buck converter mathematical model incorporates both r_L, i.e., DC resistance of the inductor, and r_C, i.e., Equivalent Series Resistance (ESR) of the capacitor, to enhance precision during the initial design phase and analyzes the effects of parasitic losses on stability and transient behavior of the synchronous buck DC-DC converter [15].

2.1. State Equations of Synchronous Buck DC-DC Converter with Non-Idealities

The state equations mathematically represent how the state variables change over time in response to variations in the input voltage, output load, and control signals. These equations are of significant importance as they provide valuable insight into the performance characteristics of the converter, such as efficiency, transient response, and stability.

2.1.1. During t_{on} Sub-Interval ($0 < t \leq DT$)

In the t_{on} period, the high side Q_H MOSFET switch is turned on, and the low side Q_L MOSFET switch is turned off, as shown in the linear subcircuit in Figure 2. The state equations are derived using fundamental methods of analyzing circuits, such as Kirchhoff's voltage and current laws. These equations are formulated as a linear combination of the input voltage source and the state variables, as represented in Equation 1. Through this time interval, the resultant output voltage is expressed as a linear combination of the input voltage source and state variables themselves, as given by Equation 2.

$$\left.\begin{aligned}\frac{di_{L(on)}}{dt} &= -\left(\frac{r_L}{L}+\frac{r_c R_{L(out)}}{(r_c+R_{L(out)})L}\right)i_L-\left(\frac{R_{L(out)}}{(r_c+R_{L(out)})L}\right)v_c+\frac{V_{in}}{L}\\ \frac{dv_{c(on)}}{dt} &= \left(\frac{R_{L(out)}}{(r_c+R_{L(out)})C}\right)i_L-\left(\frac{1}{(r_c+R_{L(out)})C}\right)v_c\end{aligned}\right\} \quad (1)$$

$$V_{out(on)} = \left(\frac{r_c R_{L(out)}}{r_c+R_{L(out)}}\right)i_L+\left(\frac{R_{L(out)}}{r_c+R_{L(out)}}\right)v_c \quad (2)$$

2.1.2. During t_{off} Sub-Interval ($DT \leq t < T$)

In the t_{off} period, the high side Q_H MOSFET switch is turned off while the low side Q_L MOSFET switch is on, as illustrated in the equivalent linear subcircuit given in Figure 3. The state equations and output voltage through this t_{off} time interval are expressed using Equations 3 and 4, respectively.

$$\left.\begin{aligned}\frac{di_{L(off)}}{dt} &= -\left(\frac{r_L}{L}+\frac{r_c R_{L(out)}}{(r_c+R_{L(out)})L}\right)i_L-\left(\frac{R_{L(out)}}{(r_c+R_{L(out)})L}\right)v_c\\ \frac{dv_{c(off)}}{dt} &= \left(\frac{R_{L(out)}}{(r_c+R_{L(out)})C}\right)i_L-\left(\frac{1}{(r_c+R_{L(out)})C}\right)v_c\end{aligned}\right\} \quad (3)$$

$$V_{out(off)} = \left(\frac{r_c R_{L(out)}}{r_c+R_{L(out)}}\right)i_L+\left(\frac{R_{L(out)}}{r_c+R_{L(out)}}\right)v_c \quad (4)$$

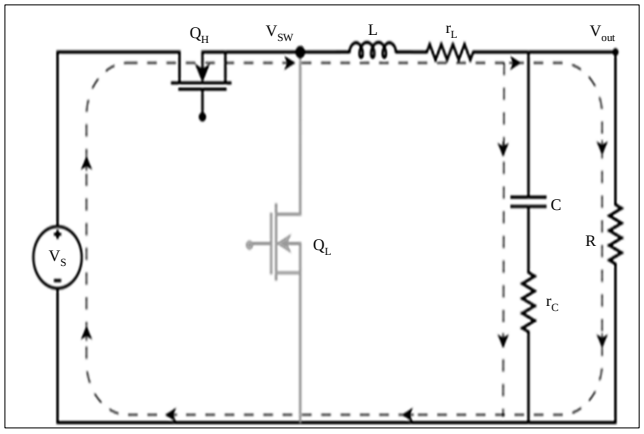

Fig. 2 Schematic of non-ideal synchronous buck converter during t_{on} subinterval

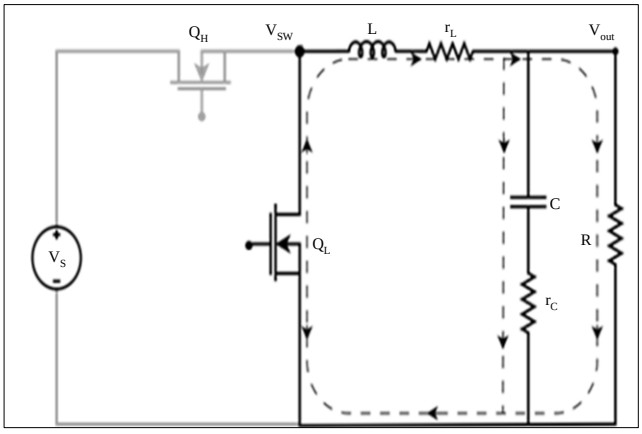

Fig. 3 Schematic of non-ideal synchronous buck converter during t_{off} subinterval

2.2. State-Space Averaging Method

State-Space Averaging (SSA) offers a mathematical approach to studying the dynamic characteristics of physical systems, including DC-DC converters. This approach utilizes input, output, and state variables represented by first-order differential equations. By averaging the state equation over a single switching cycle, this method transforms the system into a time-invariant representation suitable for deriving small-signal transfer functions and outputs [1, 16]. For DC-DC converters, state-space averaging generally relies on two fundamental equations as given by Equation 5.

$$\left.\begin{aligned}\frac{dx(t)}{dt} &= Ax(t)+Bu(t)\\ y(t) &= Cx(t)+Eu(t)\end{aligned}\right\} \quad (5)$$

According to the linear time-invariant system represented in [1, 16], the states with x vector, inputs with u vector, and outputs of the system with y vector are denoted. These vectors have dimensions of p×1, m×1, and, n×1 where p being the number of outputs, m being the number of inputs, and n being the number of states. Additionally, E, C, B, and A matrices having dimensions (p×m), (p×n), (n×m), and (n×n) respectively symbolize the input, output, dynamic, and direct-transmission matrices.

The structure of a plant, i.e., a non-ideal synchronous buck converter, is modified by switching actions of high-side and low-side MOSFETs. This alteration occurs because the circuit components are connected in different ways during each sub-interval of every switching cycle. Thus, the same circuit operates as two distinct linear circuits based on the specific switching action of the MOSFETs.

The state equations and associated matrices that describe these dynamics also vary for each sub-interval of every switching cycle. For the t_{on} time period, state matrices A_1, B_1, C_1, and E_1 representing the behavior of synchronous buck converter during ($0<t\leq DT$) are obtained using Equations 1 and 2 state equations that are given by Equation 6.

$$\left.\begin{aligned}A_1 &= \begin{bmatrix}-\left(\frac{r_L}{L}+\frac{r_c R_{L(out)}}{(r_c+R_{L(out)})L}\right) & -\frac{R_{L(out)}}{(r_c+R_{L(out)})L}\\ \frac{R_{L(out)}}{(r_c+R_{L(out)})C} & -\frac{1}{(r_c+R_{L(out)})C}\end{bmatrix}\\ B_1 &= \begin{bmatrix}1/L\\ 0\end{bmatrix}\\ C_1 &= \begin{bmatrix}\frac{r_c R_{L(out)}}{r_c+R_{L(out)}} & \frac{R_{L(out)}}{r_c+R_{L(out)}}\end{bmatrix}\\ E_1 &= [0 \quad 0]\end{aligned}\right\} \quad (6)$$

Similarly, the behaviour of a synchronous buck converter during ($DT \leq t < T$) is represented by another set of state matrices A_2, B_2, C_2, and E_2. These matrices are obtained from Equations 3 and 4 state equations are given by Equation 7.

$$\left.\begin{aligned} A_2 &= \begin{bmatrix} -\left(\frac{r_L}{L}+\frac{r_c R_{L(out)}}{(r_c+R_{L(out)})L}\right) & -\frac{R_{L(out)}}{(r_c+R_{L(out)})L} \\ \frac{R_{L(out)}}{(r_c+R_{L(out)})C} & -\frac{1}{(r_c+R_{L(out)})C} \end{bmatrix} \\ B_2 &= \begin{bmatrix} 0 \\ 0 \end{bmatrix} \\ C_2 &= \begin{bmatrix} \frac{r_c R_{L(out)}}{r_c+R_{L(out)}} & \frac{R_{L(out)}}{r_c+R_{L(out)}} \end{bmatrix} \\ E_2 &= [0 \quad 0] \end{aligned}\right\} \quad (7)$$

Next, the averaged state matrices are obtained through multiplying the state matrices of two sub-interval states with their respective duty cycle values. This results in time-weighted average matrices, representing time-invariant state variables, input and output represented by Equation 8 with bold capital letters.

$$\left.\begin{aligned} A = A_1 d + A_2(1-d) &= \begin{bmatrix} -\left(\frac{r_L}{L}+\frac{r_c R_{L(out)}}{(r_c+R_{L(out)})L}\right) & -\frac{R_{L(out)}}{(r_c+R_{L(out)})L} \\ \frac{R_{L(out)}}{(r_c+R_{L(out)})C} & -\frac{1}{(r_c+R_{L(out)})C} \end{bmatrix} \\ B = B_1 d + B_2(1-d) &= \begin{bmatrix} 1/L \\ 0 \end{bmatrix} \\ C = C_1 d + C_2(1-d) &= \begin{bmatrix} \frac{r_c R_{L(out)}}{r_c+R_{L(out)}} & \frac{R_{L(out)}}{r_c+R_{L(out)}} \end{bmatrix} \\ E = E_1 d + E_2(1-d) &= [0 \quad 0] \end{aligned}\right\} \quad (8)$$

2.3. Small Signal Modelling of the Non-Ideal Synchronous Buck DC-DC Converter

In this subsection, a small signal model of the plant, i.e., the non-ideal synchronous buck converter, is obtained by linearizing state space equations around a quiescent operating point to understand the dynamic characteristics of the plant, i.e., non-ideal synchronous buck dc-dc converter in response to small signal excitations [1, 15]. The small signal excitations refer to small disturbances around the quiescent operating point [17], as given by Equation 9.

$$\left.\begin{aligned} x(t) &= X + \hat{x}(t) \\ u(t) &= U + \hat{u}(t) \\ y(t) &= Y + \hat{y}(t) \\ d(t) &= D + \hat{d}(t) \end{aligned}\right\} \quad (9)$$

The steady-state values are denoted by uppercase bold letters, and small perturbations are represented by hat symbols above lowercase letters. Substituting these perturbations given in Equation 9 into the state-space Equation 5 yields three categories of terms: DC terms, small-signal AC terms, and second-order nonlinear terms.

On the presumption that the small-signal AC variations are significantly smaller than their steady-state counterparts ($\hat{x} \ll X$, $\hat{u} \ll U$, $\hat{y} \ll Y$, and $\hat{d} \ll D$), the non-linear terms of second order or degree are neglected. By collecting the DC components and rearranging the equations, the steady-state DC relationships are given by Equation 10.

$$\left.\begin{aligned} X &= -(A^{-1}B)U \\ Y &= -[C(A^{-1}B) - E]U \end{aligned}\right\} \quad (10)$$

The derivation of a small-signal AC representation of the plant, i.e., a non-ideal synchronous buck converter, is accomplished through recombining elements symbolized with hat terms. Following this, the Laplace transform is applied to the time-domain model, converting it into the frequency-domain, i.e., s-domain.

Following a tedious derivation, the small-signal transfer function between the control signal and output voltage is obtained for the plant, i.e., a non-ideal synchronous buck converter, incorporating the influence of non-idealities within the system. The equation is written explicitly to show how the input voltage and the system's internal states affect the output [1], as given by Equation 11.

$$\left.\begin{aligned} &\hat{y}(s) = (C[sI - A]^{-1}B + E)\hat{u}(s) + (C[sI - A]^{-1}X_d + Y_d)\hat{d}(s) \\ &with \begin{cases} X_d = \{(A_1 - A_2)X + (B_1 - B_2)U\} \\ Y_d = \{(C_1 - C_2)X + (E_1 - E_2)U\} \end{cases} \end{aligned}\right\} \quad (11)$$

Where $\hat{y}$(s) and $\hat{u}(s)$ symbolize the output and input in the s-domain, respectively, with $\hat{d}(s)$ being the small variation in duty. The matrices denoted using bold capital letters like A, B, C, and E embody the system dynamics of steady state.

In contrast, the first set of matrices A1, B1, E1, C1, and the second set of matrices A2, B2, E2, and C2 represent the small signal approximations of on and off states, respectively and letter I signifies the identity matrix. Thus, the output of the plant, i.e., a small signal averaged model of a non-ideal synchronous buck dc-dc converter, assuming that the only disturbance in the system is the change in duty cycle, can be expressed by Equation 11.

Substituting all the matrices specified in the output from the previously computed values and simplification results in the generalized small signal output transfer function given by Equation 12.

$$\frac{\hat{y}(s)}{\hat{d}(s)} = V_{in}\left(\frac{R_{L(out)}}{r_c+R_{L(out)}}\right) * \left[\frac{(1+sCr_c)}{1+\left(\frac{L+C\left[r_c R_{L(out)}+r_L(r_c+R_{L(out)})\right]}{r_L+R_{L(out)}}\right)s+\left(\frac{LC(r_c+R_{L(out)})}{r_L+R_{L(out)}}\right)s^2}\right] \quad (12)$$

Equation 12 represents the derived output transfer function of the plant, i.e., a non-ideal synchronous buck converter. This function exhibits a second-order system structure [2], characterized by two poles situated at the output filter's resonant frequency and a single zero due to the combined effect of the output C_{out} capacitor and its equivalent series resistance (r_C) given by Equation 13.

$$G_{vd}(s) = G_{do}\left[\frac{\left(1+\frac{s}{w_z}\right)}{1+\frac{s}{Qw_o}+\left(\frac{s}{w_o}\right)^2}\right] \quad (13)$$

Compare Equations 12 with 13 in order to obtain DC gain of the power stage G_{do} represented using Equation 14, W_z, i.e., zero on s-plane in the left half due to esr resistance of output capacitor represented using Equation 15, W_0 the undamped frequency of the resonant poles represented using Equation 16, and Q the quality factor of the synchronous buck converter including all the non-idealities is given by Equation 17.

$$G_{do} = V_{in}\left(\frac{R_{L(out)}}{r_c+R_{L(out)}}\right) \quad (14)$$

$$w_z = \frac{1}{Cr_c} \quad (15)$$

$$w_o = \sqrt{\frac{r_L+R_{L(out)}}{(r_C+R_{L(out)})LC}} \quad (16)$$

$$Q = \sqrt{\frac{LC(r_{L+}R_{L(out)})(r_C+R_{L(out)})}{L+C[r_CR_{L(out)}+r_L(r_C+R_{L(out)})]}} \quad (17)$$

$$G_{vd}(s) = \frac{1740(s+2273.25\times10^3)}{s^2+9374s+2.078\times10^8} \quad (18)$$

If the circuit parameters from Table 1 are substituted into the control-to-output non-ideal synchronous buck converter transfer function given in Equation 12, a numerical expression is obtained, as represented by Equation 18. This expression defines the plant, i.e., non-ideal synchronous buck converter under specified operating conditions of V_{in}=19V, V_{out}=5V, and duty cycle=0.42, i.e., subjected to open-loop frequency response analysis using a Bode plot.

Table 1. Specifications of the synchronous buck converter

Description	Parameter	Value
Input Voltage	V_{IN}	(14 -24) Volts
Output Voltage	V_{OUT}	5 Volts
Output Ripple Voltage	ΔV_{OUT}	2% (100 mV)
Inductor Current Ripple	ΔI_L	215 mA
Switching Frequency	f_{sw}	100 kHz
Inductor	L/r_L	220µH/0.05Ω
Capacitor	C/r_c	20µH/0.2Ω

The Bode plot in Figure 4 displays the frequency response of an open-loop plant, i.e., a non-ideal synchronous buck dcc-dc converter [1, 2], generated with the help of the transfer function given by Equation 18. This plot visually represents both the magnitude and phase changes of the converter's output voltage response corresponding to varying input frequencies. The solid blue line represents the frequency response of an ideal buck converter, which assumes perfect components with no losses (r_C=0, r_L=0). In contrast, the dashed red line represents the frequency response of the open-loop plant model, i.e., a non-ideal converter with included parasitic losses. Upon comparing both, it is evident that the non-ideal converter exhibits increased damping, particularly around the double pole frequency, and a reduced bandwidth due to the shift in the gain crossover frequency.

At high frequencies, the zero due to the output capacitor and its ESR resistance causes a positive phase shift. It also indicates an unlimited Gain Margin (GM) and a Phase Margin (PM) of around 9 degrees at a crossover frequency of 63.82 radians per second, which is approximately equivalent to 10.2 kilohertz. The Bode plot clearly indicates that the non-ideal synchronous buck converter has a very small phase margin. In essence, a small phase margin typically results in a poor transient response with a large overshoot.

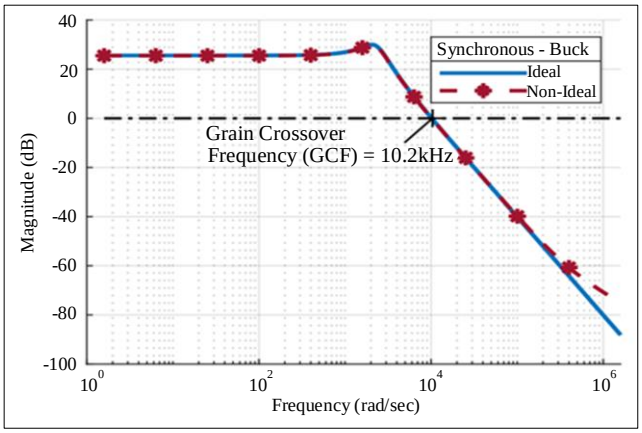

(a)

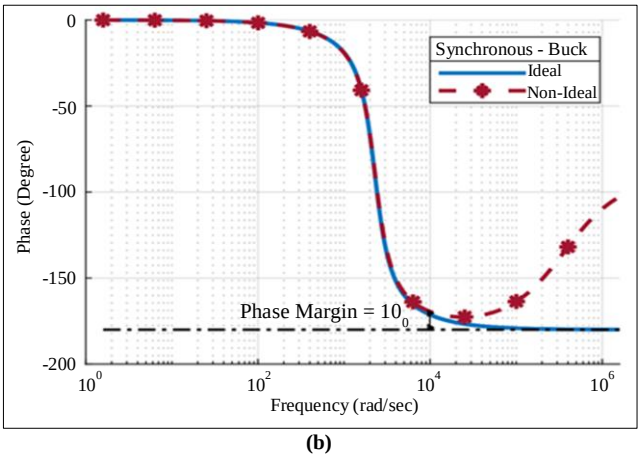

(b)

Fig. 4 Open-loop frequency response of non-ideal synchronous buck converter (a) Magnitude plot, and (b) Phase plot.

Furthermore, whether it is an ideal or non-ideal buck converter, there are no poles in the origin of the transfer function given an open-loop plant, classifying it as a type-0 system. The implication of being a type-0 system is that a non-ideal synchronous buck converter will exhibit a constant steady-state error in output voltage response to a step variation in input voltage or output load.

Indeed, the small phase margin and non-zero steady-state error both pose significant challenges in controlling buck converters. These issues are typically addressed by employing feedback control approaches, such as PID control, which will be discussed in the following section.

3. Controller Design for Voltage Mode Control of Non-Ideal Synchronous Buck Converter

3.1. Design of PID Controller

The feedback PID controller is a crucial component in the voltage mode control of the plant, i.e., a non-ideal synchronous buck dc-dc converter. Its primary objective is to adjust the conduction duration, i.e., the duty cycle of the MOSFET switches in a synchronous buck DC-DC converter to regulate the output response voltage.

Basically, the feedback PID controller's primary mission is to ensure the stability of the output response voltage. It achieves this by continuously monitoring the output voltage and comparing it to a predefined reference voltage. If a discrepancy is detected, the controller adjusts the operational periods of the device's switches to align the output voltage with the target. [18].

PID controller helps maintain system stability by minimizing the error over time, which is crucial in dynamic systems like a non-ideal synchronous buck converter where load conditions can change rapidly. Effectively managing these changes ensures that the output voltage remains within desired limits, thereby enhancing system performance. A typical PID controller's time domain mathematical representation is given by Equation 19.

$$u(t) = K_c \left[e(t) + \frac{1}{T_i} \int_0^{\tau} e(\tau) d\tau + \frac{de(t)}{dx} \right] \qquad (19)$$

Where error signal e(t) feed as input to PID controller, i.e., the difference between response output of the plant and predefined reference input signal as provided by e(t) = r(t)-y(t). The scaling factor K_c determines the PID controller's immediate response to current error e(t), the integral time (T_i) defines the speed at which the controller reacts to the built-up or accumulated error, and the derivative time (T_d) determines how fast or swiftly the controller responds to the deviation of the error signal. Now, let us take the Laplace transform of Equation 19 for s-domain representation of the PID controller output as represented by Equation 20.

$$U(s) = \left[K_p + \frac{K_i}{s} + K_d s \right] E(s) \qquad (20)$$

Where, U(s) is the output signal of a PID controller that is expressed as a weighted sum of the products of error signal E(s) with three individual scaling factors K_c, T_i, and T_d, resulting in the K_p=K_c (proportional gain), K_i=K_c/T_i (Integral gain), and K_d=K_c*T_d (Derivative gain) respectively [18], the functionality of the feedback PID controller is solely influenced by its three gain parameters, each of which has a distinct and well-understood influence on its behavior.

However, when the plant is like a DC-DC converter that is expected to encounter rapid changes in the error signal, derivative action can be beneficial as it provides a quicker response to changes in the error signal, thus allowing faster recovery from disturbances without excessive oscillations or instability compared to using only PI control. Therefore, for optimal performance in a non-ideal synchronous buck converter, including derivative gain becomes essential, as discussed in the next subsection.

3.2. Significance of PID Controller with Derivative Filter

In Voltage-Mode Control (VMC) of plant, i.e., non-ideal synchronous buck dc-dc converters, PID is critical in regulating the output response. However, the ripple in the output response due to the Equivalent Series Resistance (r_C) of the capacitor can significantly impact the derivative term of the PID controller, especially during large-signal transients since the ripple in the output parameter can introduce significant noise into the closed-loop feedback system.

This results in degraded closed-loop bandwidth and phase margin. A solution to address this noise issue is to utilize a PID controller with a dedicated derivative filter [18]. Figure 5 shows a PID controller with the filtered derivative term in a closed-loop configuration along with a plant, i.e., a non-ideal synchronous buck converter.

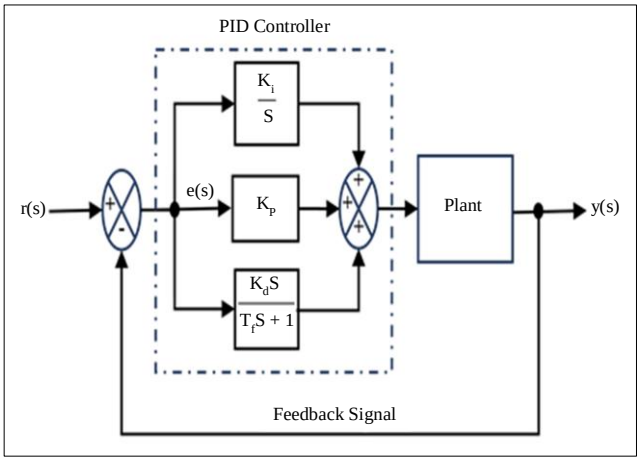

Fig. 5 Synchronous buck converter in the closed loop configuration with PID controller

The derivative filter functions as a first-order low-pass filter, attenuating the high-frequency elements and mitigating the impact of the output voltage fluctuations. The s-domain representation of a typical PID controller with a derivation filter is given by Equation 21.

$$\mathbf{G_p(s) = K_p + \frac{K_i}{s} + \frac{sK_d}{sT_f+1}} \quad (21)$$

4. Magnitude Optimum Multiple Integration (MOMI) Tuning Method

4.1. The Concept of Magnitude Optimum (MO) through the Multiple Integration (MI) Method

The MOMI tuning method [14] uses a nonparametric time domain approach with multiple integrations of plant, i.e., non-ideal synchronous buck converter input and output signals to calculate the PID controller's three gain parameters in order to satisfy "Magnitude Optimum (MO)" criteria. The "Magnitude Optimum (MO)" criterion aims to attain a close unity gain characteristic over a desired frequency range for the given plant, i.e., a non-ideal synchronous buck converter.

This is achieved by minimizing the deviation of the closed-loop magnitude frequency response of the converter output to the set point or reference input across a given bandwidth [19]. This technique is also called "Modulus Optimum" [19] or "Betragsoptimum" [7, 20].

In other words, the MO criteria seek to achieve a closed-loop system with a high bandwidth, zero phase shift, and unity gain at low frequencies. These characteristics are desirable for many control applications, as they allow the control system to track reference inputs and reject disturbances quickly and accurately.

The original Magnitude Optimum (MO) criteria present significant challenges due to its requirement for estimating an extensive quantity of process parameters, even when it comes to PID controllers characterized by only three gain parameters. The MOMI method overcomes this limitation through the application of the "moments" concept, known from identification theory [21, 22] which are multiple integrals of the plant, i.e., DC-DC converter input as well as output time-responses, to parameterize the given plant, i.e., non-ideal synchronous buck converter and calculate PID controller gain parameters.

These moments provide valuable insights into the dynamic properties of plants without the need for an explicit physical plant model. In the context of the MOMI method, the moment determines the area under the curve of the output and input signals of a plant. When the plant is subjected to step change during its steady state operating conditions, this area, often referred to as the 'characteristic area', is determined by integrating the plant's output over a period equal to the settling time after all transients have disappeared.

Alternatively, if the transfer function of the plant, i.e., non-ideal synchronous buck converter, is known, the moments can be calculated straight from the coefficients of the plant's transfer function. This equality arises considering the fact that the transfer function encapsulates the connection of input with the output of a process or plant [23, 24].

4.1.1. Systematic PID Controllers Tuning Procedure: A MOMI Approach

This section explains a well-organised procedure designed to identify three PID controller gain parameters using the MOMI method in four distinct stages. First, let us obtain the plant, i.e., non-ideal synchronous buck converter transfer function in a rational polynomial form as represented by Equation 22.

$$G_p(s) = K_{pr}\left(\frac{1+b_1s+b_2s^2+\ldots\ldots\ldots+b_ms^m}{1+a_1s+a_2s^2+\ldots\ldots\ldots+a_ns^n}\right)e^{-sT_d} \quad (22)$$

In the second step, compute the moments directly using the co-efficient of the denominator as well as the numerator of the plant, i.e., non-ideal synchronous buck converter transfer function as given in Equation 18 according to the MOMI tuning procedure specified in [18, 23] as follows.

$$\left.\begin{aligned} A_0 &= K_{pr} \\ A_1 &= K_{pr}(-(b_1 - a_1) + T_d) \\ A_2 &= K_{pr}\left(-(a_2 - b_2) - T_d b_1 + \frac{T_d^2}{2!}\right) + A_1 a_1 \\ A_k &= K_{pr}\left((-1)^{k+1}(a_k - b_k) + \left(\sum_{i=1}^{k}(-1)^{k+i}\frac{T_d^i * b_{k-i}}{i!}\right)\right) \\ &\quad + \sum_{i=1}^{k-1}(-1)^{k+i-1}A_i a_{k-i} \end{aligned}\right\} \quad (23)$$

In the MOMI tuning method, initially, the PID controller's gains are calculated with T_F=0 substitution in the Equation 24, and then the moments obtained through this procedure are used to determine a PID controller without the derivative filter. Next, the second iteration focuses on refining the behavior of the first-order derivative filter through adjusting the time constant T_f as given in Equation 24 based on a numerical constant N, which typically ranges from 8 to 20 [14].

$$T_F = \frac{K_d}{(N \times K_p)} \quad (24)$$

In the third step, to simplify the subsequent mathematical analysis, the first-order filter within the PID controller is integrated into the plant model as per the MOMI tuning method.

This allows for a more efficient calculation of the controller moments, which are subsequently re-evaluated using Equation 25, incorporating the previously determined filter time constant.

$$\left.\begin{aligned} A^* &= A_0 \\ {A_1}^* &= A_1 + A_0 T_F \\ {A_2}^* &= A_2 + A_1 T_F + A_0 {T_F}^2 \end{aligned}\right\} \quad (25)$$

Where A_i^* symbolize moments as stipulated in the MOMI tuning method with 1st order derivative filter as part of the plant transfer function. Finally, the moments computed in the last step are expressed in a compact matrix representation to determine the PID controller gain parameter as given by Equation 26.

$$\begin{bmatrix} K_I \\ K_P \\ K_D \end{bmatrix} = \begin{bmatrix} -{A_1}^* & {A_0}^* & 0 \\ -{A_3}^* & {A_2}^* & -{A_1}^* \\ -{A_5}^* & {A_4}^* & -{A_3}^* \end{bmatrix} \begin{bmatrix} -0.5 \\ 0 \\ 0 \end{bmatrix} \quad (26)$$

The transfer function of the plant, i.e., non-ideal synchronous buck converter, as represented numerically by Equation 18, is compared with Equation 22 to identify key parameters of the plant, i.e., non-ideal synchronous buck converter as required by the MOMI method [25].

These parameters include DC gain (K_{pr}=1720), numerator (b_1=2273.25×10^3), and denominator (a_1=9374, a_2=2.078×10^8) coefficients. The time delay T_d is assumed to be zero to simplify computations, as it is negligibly small. The MOMI tuning method is then applied to calculate the first five moments (A0, A1, A2, A4, A5) incorporating K_{pr}, T_d, and transfer function coefficients as defined by Equation 23.

These moments serve as quantitative representations of the system's dynamic behavior. With the time constant of derivative filter T_f made equal to zero, the initial values of the three PID controller gain (K_p, K_i, K_d) are estimated. In subsequent iterations, the T_f, i.e., the derivative filter time constant, is calculated using the parameters obtained during the first iteration, where N being a numerical constant typically ranging from 8 to 20 [14].

Once the value of T_f is found, it is substituted in the Equation 26 to obtain $K_i \approx 1697$, $K_p \approx 0.03933$, $K_d \approx 2.848\times10^{-6}$ with $T_f = 1.216\times10^{-5}$ for the design. The s-domain representation of the transfer function of the PID controller optimized using the MOMI tuning method is given by Equation 27.

$$G_{C\_MOMI}(s) = \frac{2.848e{-}06s^2 + 0.03833s + 1697}{1.216e{-}05s^2 + s} \quad (27)$$

4.2. Damped Oscillation Method of PID Controller Tuning

The classic PID controller tuning approach of Damped oscillation, as an alternative to the traditional Ziegler-Nichols tuning method [26], provides a safer technique by preventing systems from reaching marginally stable states, thereby avoiding potentially irreversible damage. In contrast, the damped oscillation method for tuning PID controllers begins by setting the controller to proportional mode, which means both integral and derivative gains are zero. The closed-loop with P-only (proportional) gain controller is incrementally decreased or increased until the system's response exhibits a predetermined decay ratio between two consecutive peaks [6, 26].

At this moment, the proportional gain and period of the oscillation, which are damped in nature with respect to the original, are used to calculate the final PID parameters. This method represents PID controllers with T_f=0, in spite of which they ensure a balance between system responsiveness and stability [27].

4.2.1. The Harriot Method

The Harriot method, introduced by P.R. Harriot in 1966, is one such method [10]. It starts by incrementally adjusting the proportional gain in a closed-loop with the plant, i.e., non-ideal synchronous buck converter until a quarter decay ratio is achieved between consecutive peaks [28].

That specific K_{pd} (proportional gain) and T_{ud} (period of damped oscillation) between consecutive peaks are needed to compute the PID controller gain parameters. The proportional gain is calculated as K_p=K_{pd}, the integral time as T_i=T_{ud}/1.5, and the derivative time as T_d=T_i/6.

The s-domain representation of the transfer function of the PID controller optimized using the Harriot tuning method [10] is expressed by Equation 28.

$$G_{C\_Harriot}(s) = \frac{1.2237e{-}06s^2 + 0.126s + 138.102}{s} \quad (28)$$

4.2.2. The Good-Gain Method

It is an alternative approach developed by Finn Haugen and falls within the category of damped oscillation techniques. [28]. It begins by incrementally adjusting the proportional gain until the response curve exhibits a simple overshoot and little observable undershoot [28].

That specific K_{PGG} (proportional gain) and T_{ud} (period of damped oscillation) are needed to compute feedback PID controller gain values. The integral time, proportional gain, and derivative time are calculated according to the specified rule as follows: K_p=0.8×K_{PGG}, T_i=1.5×T_{ud}, and T_d=0.25×T_i, respectively [29]. The s-domain representation of the transfer function of the PID controller optimized using the Good-Gain tuning method [29] is given by Equation 29.

$$G_{C\_GoodGain}(s) = \frac{2.4523e{-}06s^2 + 0.1042s + 17.65}{s} \quad (29)$$

The Bode plot in Figure 6 presents the open-loop as well as the closed-loop frequency response of the plant with a PID controller optimized using three distinct tuning methods.

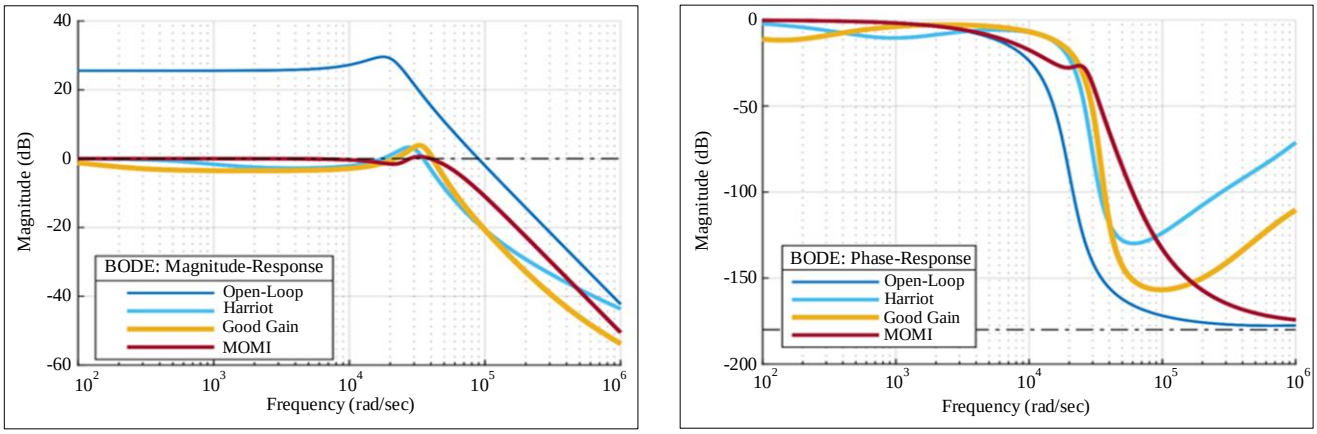

(a) **(b)**

Fig. 6 The closed-loop frequency response of non-ideal synchronous buck converter with PID controller optimized using different tuning methods (a) Magnitude response, and (b) Phase response.

Table 2. Specifications of the synchronous buck converter

Parameters	Open-Loop Standalone System	MOMI Method	Harriot Method	Good-Gain Method
Rise Time	68.1 µsec	39.1 µsec	59.6.1 µsec	55.7.1µsec
Settling Time	0.69 msec	0.40 msec	4.36 msec	31.2 msec
Overshoot	33%	3.46%	3.97%	0
GCF (Bandwidth)	14.2 kHz	6.32 kHz	5.59 kHz	6.57 kHz
Phase Margin	9 degrees	115 degrees	74.9 degrees	53.9 degrees
GM (Peak)	29.6 dB	1 dB	3.33 dB	3.86 dB
PCF	2.82 kHz	5.19 kHz	4.37 kHz	5.25 kHz
Stability	Yes	Yes	Yes	Yes
Complexity	NaN	Medium	Low	Low

The Bode plot comprises two components: the Magnitude Plot and the Phase Plot. The Magnitude Plot reveals how the controllers amplify or attenuate signals across various frequencies. Initially, all control methods exhibit similar gains at lower frequencies. However, as the frequency increases, a divergence in performance becomes evident. Notably, the MOMI-PID and Harriot-PID exhibit more attenuation at higher frequencies.

The phase plot depicts the phase shift introduced by each controller measured at the gain crossover frequency. Among the methods, the MOMI-PID demonstrates the highest Phase margin. Table 2 provides numerical data extracted from both phase and magnitude plots of the Bode plot. This data serves as a valuable resource for further analysis and interpretation of the performance of each tuning method.

The Table 2 provides a comprehensive analysis of three different tuning methods encapsulating closed-loop control performance: the MOMI Method, Harriot Method, and Good-Gain Method, in contrast to the open-loop standalone system.

The performance of these methods is evaluated based on several parameters, including rise time, settling time, overshoot, Gain Crossover Frequency (GCF), phase margin, Gain Margin (GM), Phase Crossover Frequency (PCF), stability, and the complexity of the tuning method.

The Open-loop standalone system exhibits the largest values for rise time, settling time, overshoot, and GCF. Nevertheless, it also has the smallest values for phase margin and GM.

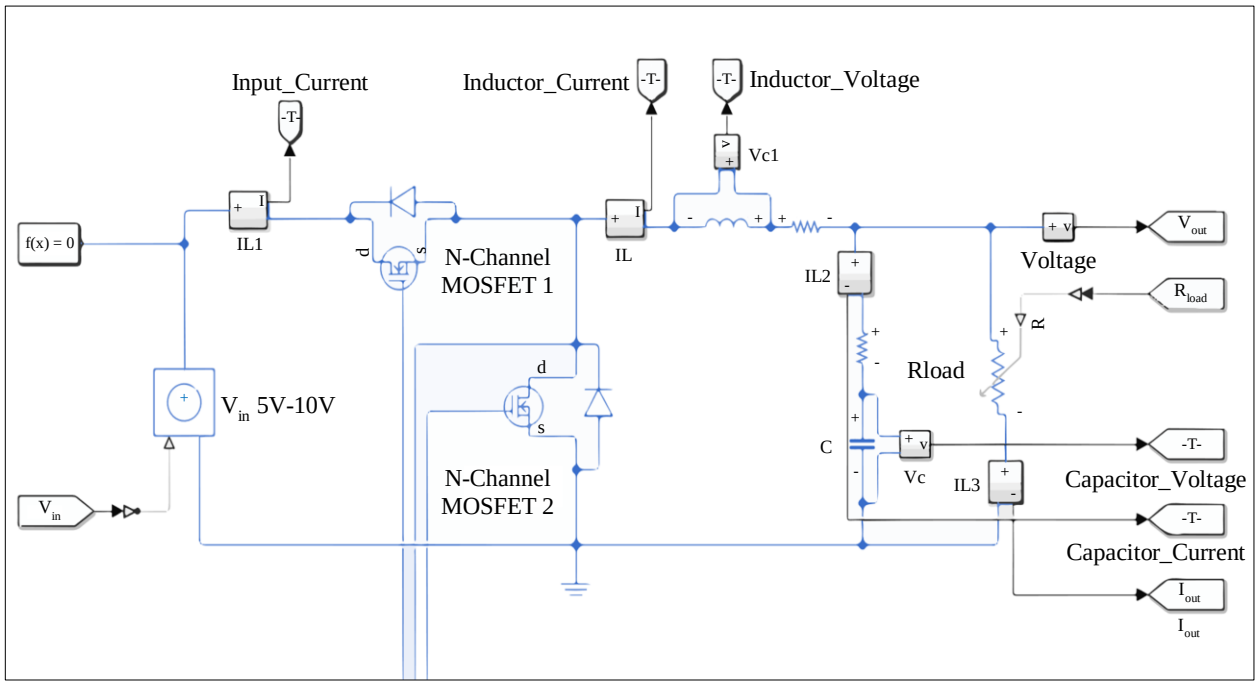

Fig. 7 System-level model of a non-ideal synchronous buck converter with PID controller in the closed-loop

These parameters act as the reference for comparing the performance of closed-loop systems optimized through different tuning methods. The MOMI method shows a significant enhancement in rise time as well as settling time compared to the standalone open-loop system. It also has a much lower overshoot and the highest phase margin. However, the GCF and GM are lower, and the method is confirmed to be stable. The complexity of the tuning method is medium. The Harriot method has improved rise time as well as settling time, compared to the Good-Gain method. The overshoot is slightly higher than the MOMI method, but the GCF is lower. The phase margin, GM, and PCF are all within acceptable ranges, and the method is confirmed to be stable. The complexity of the tuning method is low.

The Good-Gain method has the highest values for rise time as well as settling time among the four methods. However, it is the only method that has achieved zero overshoot. The GCF, phase margin, GM, and PCF are all within acceptable ranges, and the method is confirmed to be stable. The complexity of the tuning method is low. This comparison allows design engineers to make knowledgeable decisions when selecting the most suitable tuning method for their specific control system requirements.

5. Results and Discussions

5.1. Simulation of Closed-Loop Non-Ideal Synchronous Buck Converter with PID Controller

This section explores the feasibility and effectiveness of employing a Proportional-Integral-Derivative (PID) controller in closed-loop voltage mode control for regulating the output voltage response of the plant, i.e., a non-ideal synchronous buck converter. The discussion will include theoretical considerations validation through simulations.

The significance lies in using Simscape Electrical for simulating the closed-loop system, which allows for modelling non-ideal behavior such as inherent DC resistance and ESR of components like inductors and capacitors, as well as finite on-resistance of MOSFET switches leading to voltage drops and power losses.

The Simscape Electrical of the Simulink/MATLAB environment provides dedicated electrical component libraries to model these non-ideal effects. Simscape Electrical is a domain-specific language that provides a library of electrical components for modelling and simulating electrical systems [30, 31].

Figure 7 illustrates a system-level model of a non-ideal synchronous buck converter employing a PID controller for voltage mode control in the closed-loop configuration within the Simulink environment. The simulation of plant, i.e., non-ideal synchronous buck dc-dc converter under predefined designs specific operating conditions of V_{in}=19V, V_{out}=5V, and duty cycle d=0.42 meets the design specification as a standalone system in open-loop [32] as specified in Table 1.

Figure 8 shows that the inductor ripple current is well within 215mA, which was the given design constraint initially. The output ripple voltage is also well within 2% (100mV), which was the major objective of the design, as shown in Figure 9.

After meeting the design specifications constraint provided in Table 1, the performance and robustness of the PID controller optimized through the MOMI, Harriot, and Good-Gain tuning methods are tested individually. The closed-loop system is subjected to three different conditions: input voltage variations, output load variations, and output voltage set-point/reference variations [33].

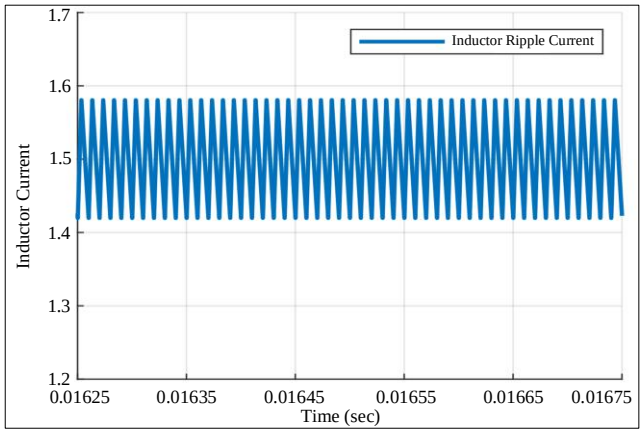

Fig. 8 Inductor current ripple ΔI_L of standalone synchronous buck converter in the open-loop

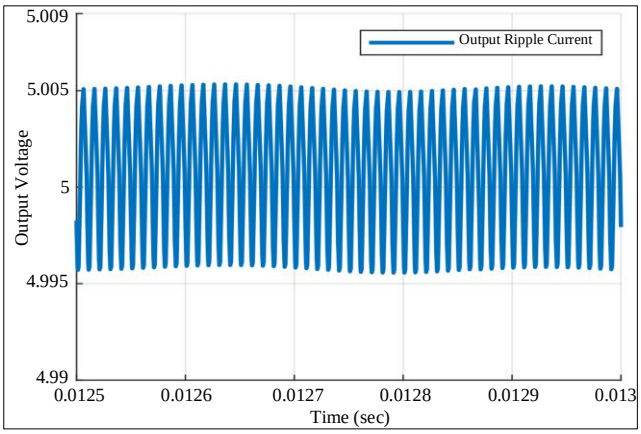

Fig. 9 Output voltage ΔV_{OUT} of standalone synchronous buck converter in the open-loop

5.2. Transient Response under Input Voltage Variations

5.2.1. Output Response to 25% Step Increase in Input Voltage

The performance of the PID controller was optimized with MOMI, Harriot, and Good-Gain tuning methods to achieve voltage mode control of the plant. .i.e., a non-ideal synchronous buck converter for 25% step input voltage variation is illustrated in Figure 10.

The MOMI method shows a small overshoot of only 10%, a quick settling time of 1.8 milliseconds, and no steady-state error. The Harriot method shows a significant overshoot of 26%, a longer settling time of over 20 milliseconds, and a steady-state error of 3%.

The Good-Gain method shows a considerable overshoot of 26%, an extended settling time of over 20 milliseconds, and a non-negligible steady-state error of 4%. In summation, under a 25% source input voltage variation, the MOMI method appears to outperform the Harriot and Good-Gain methods in terms of steady-state error, settling time, and overshoot.

5.2.2. Output Response to 33% Step Increase in Input Voltage

In comparing three PID controller tuning methods - MOMI, Harriot, and Good-Gain under 33% step input voltage variation, the subsequent observations could be made with the closed-loop response as represented in Figure 11. The MOMI method showed a slight increase in overshoot to 14% but maintained the same settling time of 1.8 milliseconds and had no steady-state error.

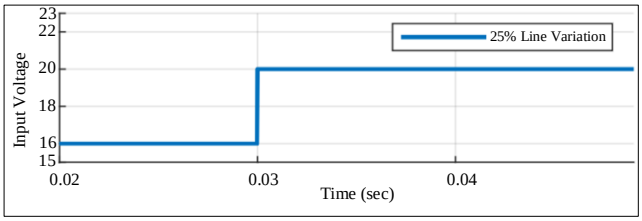

(a)

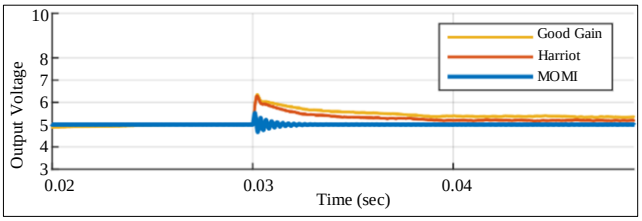

(b)

Fig. 10 Performance of PID controller tuning methods for 25% variation in the source input voltage (a) Input voltage, and (b) Output voltage.

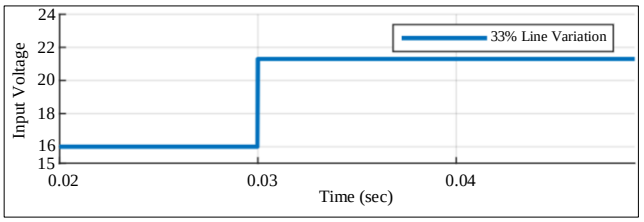

(a)

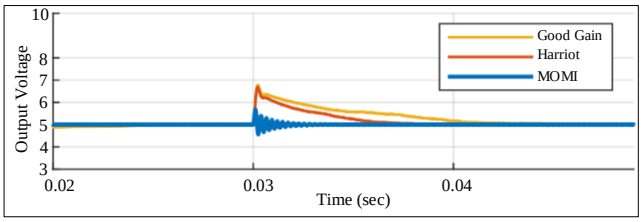

(b)

Fig. 11 Performance of PID controller tuning methods for 33% variation in the source input voltage (a) Input voltage, and (b) Output voltage.

The Harriot method had an increased overshoot of 34% but a reduced settling time of 7.7 milliseconds and no steady-state error. The Good-Gain method had an increased overshoot of 36%, a reduced settling time of 14.3 milliseconds, and no steady-state error.

All three methods eliminate the steady-state error under 33% step input voltage variation. However, under these circumstances, the MOMI method still has negligible overshoot and settling time.

5.2.3. Output Response to a 50% Step Increase in Input Voltage

Further evaluation of three PID controller tuning methods - MOMI, Harriot, and Good-Gain- is conducted under a 50% source input voltage variation for the plant. i.e., non-ideal synchronous buck converter, the subsequent observations could be made as given in Figure 12.

The MOMI method experienced a minor increase in overshoot to 16%, while the settling time increased to 2.7 milliseconds with zero steady-state error. Both Harriot and Good-Gain methods saw an extensive overshoot increase to 50% and 54%, respectively, but achieved a substantial settling time of 11 milliseconds and 16.4 milliseconds with no steady-state error.

In conclusion, all three methods successfully eliminate the steady-state error under a 50% source input voltage variation. Still, the MOMI method demonstrated better overshoot and settling time under these extreme conditions.

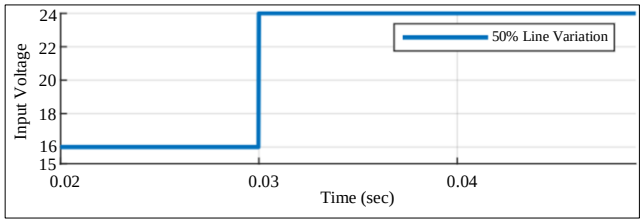

(a)

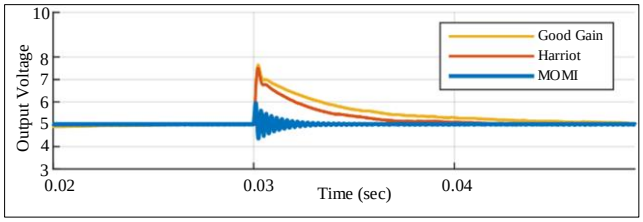

(b)

Fig. 12 Performance of PID controller tuning methods for 50% variation in the source input voltage (a) Input voltage, and (b) Output voltage.

5.3. Transient Response under Output Load Variations

5.3.1. Output Response to 20% Step Increase in Output Load

When evaluating three PID controller tuning methods - MOMI, Harriot, and Good-Gain under a 20% output load variation for the plant, i.e., non-ideal synchronous buck converter, the subsequent observations could be made as given in Figure 13.

The MOMI Method had a slight overshoot of 10% and a minimal settling time of 0.5 milliseconds, with no steady-state errors. Both Harriot and Good-Gain methods experienced small undershoots of -1% and -2%, respectively, but with significant settling times of 6 and 10 milliseconds under zero steady-state error.

In conclusion, all three methods removed the steady-state error under a 20% output load variation. Still, the MOMI method had the smallest overshoot and least settling time among all the methods.

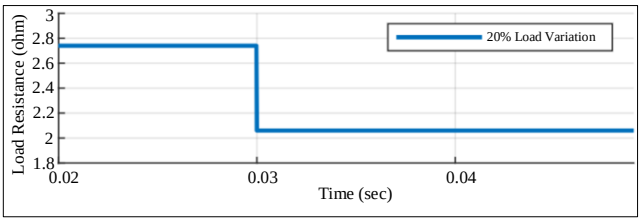

(a)

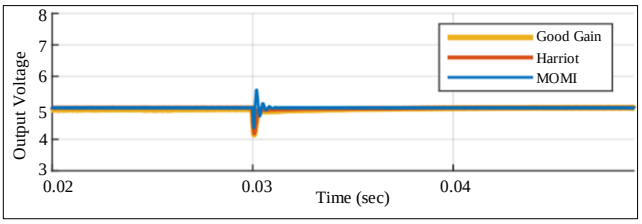

(b)

Fig. 13 Performance of PID controller tuning methods for 20% variation in the output load (a) Input voltage, and (b) Output voltage.

5.3.2. Output Response to 33% Step Increase in Output Load

When evaluating three PID controller tuning methods - MOMI, Harriot, and Good-Gain under a 33% output load variation for the plant, i.e., non-ideal synchronous buck converter, the subsequent observations shall be made as given in Figure 14.

The MOMI method increased overshoot by 18% and maintained a very small settling time of 0.8 milliseconds, having zero steady-state error. Both Harriot and Good-Gain methods experienced a small increase in the undershoot of -4% and -5%, respectively, but with a decreased settling time of 3 milliseconds and 4 milliseconds with no steady-state error.

In conclusion, all three methods removed the steady-state error under a 33% output load variation. Still, the MOMI method had the smallest overshoot and least settling time among all the methods.

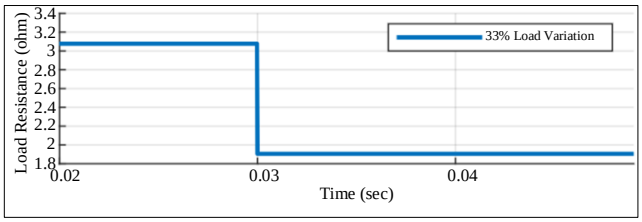

(a)

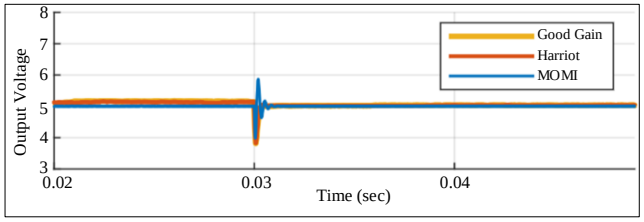

(b)

Fig. 14 Performance of PID controller tuning methods for 33% variation in the output load (a) Input voltage, and (b) Output voltage.

5.3.3. Output Response to 50% Step Increase in Output Load

Further evaluating three PID controller tuning methods - MOMI, Harriot, and Good-Gain under a 50% output load variation for the plant, i.e., non-ideal synchronous buck converter, the subsequent observations shall be made from Figure 15.

The MOMI method had a small increase in overshoot of 20% compared to the previous and maintained a very short settling time of 1 millisecond with no steady-state error. Both Harriot and Good-Gain methods experienced a significant increase in the undershoot of -34% and -38%, respectively, but with a decreased settling time of 2 milliseconds and 4 milliseconds with no steady-state error. In conclusion, all three methods removed the steady-state error under a 50% output load variation. Still, the MOMI method had the better overshoot and least settling time among all the methods.

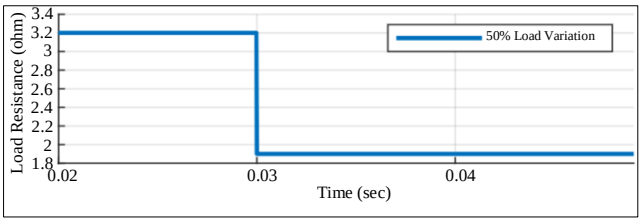

(a)

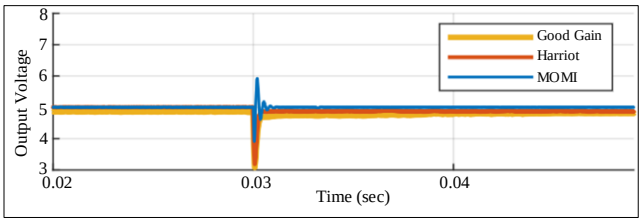

(b)

Fig. 15 Performance of PID controller tuning methods for 50% variation in the output load (a) Input voltage, and (b) Output voltage.

5.4. Tracking Performance under Output Reference Variations

To analyze the PID controller's closed-loop set-point/reference voltage tracking performance, the output reference voltage signal fed as input to the PID controller is varied between 3.3V and 5V in a square wave pattern at a frequency of 25Hz.

The lowest error signal is observed with the PID controller optimized with the MOMI tuning method, as illustrated in Figure 16. with minimal overshoot/undershoot and the fastest settling time.

While the Harriot method shows moderate error, overshoot/undershoot, and settling time compared to the MOMI method, Good-Gain experiences significant overshoot/undershoot with the slowest settling time. This suggests that the MOMI method has superior tracking capability and rapid adaptation to reference changes, making it ideal for applications demanding tight voltage control and fast transient response.

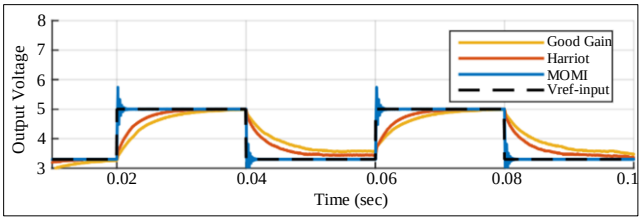

Fig. 16 Performance of PID controller tuning methods for output reference voltage variation between 3.3V and 5V

6. Conclusion

This research paper contributes to the field of control systems by providing a detailed comparative analysis of three PID controller tuning methods - MOMI, Harriot, and Good-Gain in the context of plant, i.e., non-ideal synchronous buck dc-dc converter for achieving voltage mode control.

The study utilizes a non-ideal model of the DC-DC synchronous buck converter, obtained through state space averaging and small signal modelling techniques, which provides a more accurate representation of the converter by accounting for non-idealities often overlooked in ideal models. The simulation of the plant, i.e., a non-ideal synchronous buck dc-dc converter in a closed-loop configuration with feedback PID controller, was conducted with the help of the Simscape tool in the MATLAB/Simulink environment.

This tool's ability to model physical systems and integrate them with control algorithms within a single environment was instrumental in accurately simulating the system's response to various changes. The three tuning methods were evaluated under different input voltage, output load, and output reference voltage variation conditions.

The MOMI method consistently outperformed the Harriot and Good-Gain methods in terms of undershoot, overshoot, settling time, and steady-state error across all variations. This superior performance can be attributed to the MOMI method's robustness to variations in both input voltage and output load, as well as its quick response times, making it highly effective in real-world applications where these variations are common and quick response times are crucial. In contrast, while the Harriot and Good-Gain methods were effective in eliminating the steady-state error, they exhibited significant overshoot and undershoot and longer settling times, especially under higher variations. These methods might be more suitable for applications where overshooting, undershooting, and settling time are less critical.

Furthermore, the MOMI method demonstrated superior tracking capability and rapid adaptation to reference changes, making it ideal for applications demanding tight voltage control and fast transient response. This is a significant improvement over state-of-the-art techniques or those already reported in the literature, which often struggle with these challenges.

Future research could explore the effectiveness of these tuning methods on other types of converters under different input voltage, output load, and output reference voltage variations. This could further validate the findings of this study and contribute to the development of more efficient and reliable control systems.

References

[1] Robert W. Erickson, and Dragan Maksimović, *Fundamentals of Power Electronics*, Springer New York, 2001. [CrossRef] [Google Scholar] [Publisher Link]

[2] Teuvo Suntio, Tuomas Messo, and Joonas Puukko, *Power Electronic Converters: Dynamics and Control in Conventional and Renewable Energy Applications*, 2nd ed., John Wiley & Sons, Ltd, pp. 1-720, 2017. [Google Scholar] [Publisher Link]

[3] Ke-Horng Chen, *Power Management Techniques for Integrated Circuit Design*, John Wiley & Sons, 2016. [CrossRef] [Google Scholar] [Publisher Link]

[4] Liping Guo, John Y. Hung, and R.M. Nelms, "Evaluation of DSP-Based PID and Fuzzy Controllers for DC-DC Converters," *IEEE Transactions on Industrial Electronics*, vol. 56, no. 6, pp. 2237-2248, 2009. [CrossRef] [Google Scholar] [Publisher Link]

[5] Dale E. Seborg et al., *Process Dynamics and Control*, 4th ed., John Wiley & Sons, 2010. [Google Scholar] [Publisher Link]

[6] J.G. Ziegler, and N.B. Nichols, "Optimum Settings for Automatic Controllers," *Journal of Dynamic Systems, Measurement, and Control*, vol. 115, no. 2B, pp. 220-222, 1993. [CrossRef] [Google Scholar] [Publisher Link]

[7] Karl J. Åström, and Tore Hägglund, *PID Controllers: Theory, Design, and Tuning*, 2nd ed., ISA - The Instrumentation, Systems and Automation Society, 1995. [Google Scholar] [Publisher Link]

[8] G.H. Cohen, and G.A. Coon, "Theoretical Consideration of Retarded Control," *Journal of Fluids Engineering*, vol. 75, no. 5, pp. 827-834, 1953. [CrossRef] [Google Scholar] [Publisher Link]

[9] A.R. Catheron, "Discussion: On the Automatic Control of Generalized Passive Systems (Chien, Kun Li, Hrones, J. A., and Reswick, J. B., 1952, Trans. ASME, 74, pp. 175-183)," *Journal of Fluids Engineering*, vol. 74, no. 2, pp. 183-184, 1952. [CrossRef] [Google Scholar] [Publisher Link]

[10] Oladimeji Ibrahim, Nor Zaihar Yahaya, and Nordin Saad, "Comparative Studies of PID Controller Tuning Methods on A DC-DC Boost Converter," *2016 6th International Conference on Intelligent and Advanced Systems (ICIAS)*, Kuala Lumpur, Malaysia, pp. 1-5, 2016. [CrossRef] [Google Scholar] [Publisher Link]

[11] Jan Maciejowski, *Predictive Control: With Constraints*, Pearson Education, 2002. [Publisher Link]

[12] C.C. Lee, "Fuzzy Logic in Control Systems: Fuzzy Logic Controller. I," *IEEE Transactions on Systems, Man, and Cybernetics*, vol. 20, no. 2, pp. 404-418, 1990. [CrossRef] [Google Scholar] [Publisher Link]

[13] Karl Johan Åström, and Björn Wittenmark, *Adaptive Control*, 2nd ed., Courier Corporation, pp. 1-573, 2013. [Publisher Link]

[14] Damir Vrančić, J. Stefan, and I. Slovenia, "Magnitude Optimum Techniques for PID Controllers," *Introduction to PID Controllers – Theory, Tuning and Application to Frontier Areas*, pp. 75-102, 2012. [Google Scholar] [Publisher Link]

[15] Sanjeevikumar P., Nagesh Prabhu, and Suryanarayana K., *Advances in Renewable Energy and Electric Vehicles*, 1st ed., Springer Singapore, 2022. [CrossRef] [Google Scholar] [Publisher Link]

[16] Robert Priewasser et al., "Modeling, Control, and Implementation of DC-DC Converters for Variable Frequency Operation," *IEEE Transactions on Power Electronics*, vol. 29, no. 1, pp. 287-301, 2014. [CrossRef] [Google Scholar] [Publisher Link]

[17] H. Swathi Hatwar, Ravikiran Rao M., and Suryanarayana K., "Modeling and Analysis of GaN-Based Buck Converter," *Advances in Renewable Energy and Electric Vehicles*, pp. 307-320, 2021. [CrossRef] [Google Scholar] [Publisher Link]

[18] Liuping Wang, "Closed-Loop Performance and Stability," *PID Control System Design and Automatic Tuning Using MATLAB/Simulink*, John Wiley & Sons, Ltd, pp. 31-70, 2020. [CrossRef] [Google Scholar] [Publisher Link]

[19] J.W. Umland, and M. Safiuddin, "Magnitude and Symmetric Optimum Criterion for the Design of Linear Control Systems: What is it and How does it Compare with the others?," *IEEE Transactions on Industry Applications*, vol. 26, no. 3, pp. 489-497, 1990. [CrossRef] [Google Scholar] [Publisher Link]

[20] C. Kessler, "About the Advance Calculation of Optimally Coordinated Control Loops," *Automation Technology*, vol. 3, no. 1-12, pp. 40-49, 1955. [CrossRef] [Google Scholar] [Publisher Link]

[21] F. Hli, "A General Method for Time Domain Network Synthesis," *Transactions of the IRE Professional Group on Circuit Theory*, vol. 1, no. 3, pp. 21-28, 1954. [CrossRef] [Google Scholar] [Publisher Link]

[22] Hans-Peter Preuß, "Model-Free PID-Controller Design by Means of the Method of Gain Optimum," *Automation Technology*, vol. 39, no. 1-12, pp. 15-22, 1991. [CrossRef] [Google Scholar] [Publisher Link]

[23] Damir Vrančić, Stanko Strmčnik, and Đani Juričić, "A Magnitude Optimum Multiple Integration Tuning Method for Filtered PID Controller," *Automatica*, vol. 37, no. 9, pp. 1473-1479, 2001. [CrossRef] [Google Scholar] [Publisher Link]

[24] Damir Vrančić, Youbin Peng, and Stanko Strmčnik, "A New PID Controller Tuning Method Based on Multiple Integrations," *Control Engineering Practice*, vol. 7, no. 5, pp. 623-633, 1999. [CrossRef] [Google Scholar] [Publisher Link]

[25] Sumukh Surya, Mohan Krishna Srinivasan, and Sheldon Williamson, "Modeling of Average Current in Non-Ideal Buck and Synchronous Buck Converters for Low Power Application," *Electronics*, vol. 10, no. 21, pp. 1-16, 2021. [CrossRef] [Google Scholar] [Publisher Link]

[26] Finn Haugen, "Ziegler-Nichols' Closed-Loop Method," *Tech Teach*, pp. 1-7, 2010. [Google Scholar]

[27] Kaiwei Yao, Yuancheng Ren, and F.C. Lee, "Critical Bandwidth for the Load Transient Response of Voltage Regulator Modules," *IEEE Transactions on Power Electronics*, vol. 19, no. 6, pp. 1454-1461, 2004. [CrossRef] [Google Scholar] [Publisher Link]

[28] Finn Haugen, "The Good Gain Method for PI(D) Controller Tuning," *Tech Teach*, pp. 1-7, 2010. [Google Scholar]

[29] Vanshika Jindal, and Dheeraj Joshi, "A Comparative Analysis of Classical Tuning Methods of PI Controllers on Non-Ideal Buck Converter," *2022 2nd International Conference on Power Electronics & IoT Applications in Renewable Energy and its Control (PARC)*, Mathura, India, pp. 1-5, 2022. [CrossRef] [Google Scholar] [Publisher Link]

[30] Atieh Delavari, Innocent Kamwa, and Patrice Brunelle, "Simscape Power Systems Benchmarks for Education and Research in Power Grid Dynamics and Control," *2018 IEEE Canadian Conference on Electrical & Computer Engineering (CCECE)*, Quebec, Canada, pp. 1-5, 2018. [CrossRef] [Google Scholar] [Publisher Link]

[31] Trever J. Hassell, Wayne W. Weaver, and Aurenice M. Oliveira, "Using Matlab's Simscape Modeling Environment as a Simulation Tool in Power Electronics and Electrical Machines Courses," *2013 IEEE Frontiers in Education Conference (FIE)*, Oklahoma City, USA, pp. 477-483, 2013. [CrossRef] [Google Scholar] [Publisher Link]

[32] M. Chandini Gowda, and P.B. Savitha, "Average Current Control of Buck-Boost Converter," *2022 IEEE 9th Uttar Pradesh Section International Conference on Electrical, Electronics and Computer Engineering (UPCON)*, Prayagraj, India, pp. 1-5, 2022. [CrossRef] [Google Scholar] [Publisher Link]

[33] Joshua Slough et al., "Modeling and Simulation of Electric Vehicles Using Simulink and Simscape," *2021 IEEE 94th Vehicular Technology Conference (VTC2021-Fall)*, Norman, USA, pp. 1-6, 2021. [CrossRef] [Google Scholar] [Publisher Link]